GIP analogues augment bone strength by modulating bone composition in diet-induced obesity in mice

Sagar Vyavahare, Aleksandra Mieczkowska, Peter Flatt, Daniel Chappard, Nigel Irwin, Guillaume Mabilleau

GIP analogues augment bone strength by modulating bone composition in diet-induced obesity in mice

Sagar S Vyavahare[1], Aleksandra Mieczkowska[2], Peter R Flatt[1], Daniel Chappard[2,3,4], Nigel Irwin[1], Guillaume Mabilleau[2,3,4]

[1] School of Biomedical Sciences, University of Ulster, Coleraine, Northern Ireland, United Kingdom

2 Groupe Etudes Remodelage Osseux et biomatériaux, GEROM, UPRES EA 4658, UNIV Angers, SFR ICAT 4208, Institut de Biologie en Santé, Angers, France

[3] Service Commun d'Imagerie et Analyses Microscopiques, SCIAM, UNIV Angers, SFR ICAT 4208, Institut de Biologie en Santé, Angers, France

[4] Bone Pathology Unit, Angers University hospital, 49933 Angers Cedex, France

Please send all correspondence to:

Guillaume Mabilleau, PhD
GEROM-LHEA UPRES EA 4658
Institut de Biologie en Santé
Université d'Angers
4 rue larrey
49933 Angers Cedex 09
France

☎ : +33(0) 244 688 450
Fax : +33(0) 244 688 451
✉ : guillaume.mabilleau@univ-angers.fr

Abstract word count: 250 words

Manuscript word count: 4104 words

Number of references: 50

Number of Figures: 5

Number of tables: 1

Short running title: GIP in diet-induced obesity and diabetes

DISCLOSURE

None of the authors has any conflict of interest to report

doi: 10.1016/j.peptides.2019.170207

Highlights

- (D-Ala^2)-GIP and (D-Ala^2)-GIP-Tag had similar biological effects in vitro
- (D-Ala^2)-GIP and (D-Ala^2)-GIP-Tag reduced non-fasting blood glucose
- (D-Ala^2)-GIP and (D-Ala^2)-GIP-Tag enhanced ultimate load and work-to-fracture
- (D-Ala^2)-GIP and (D-Ala^2)-GIP-Tag improved bone tissue material properties

ABSTRACT

Receptors to glucose-dependent insulinotropic polypeptide (GIP), have been identified on bone and GIP receptor (GIPr) knockout mice exhibit reduced bone strength and quality. Despite this, little is known on the potential beneficial bone effects of exogenous GIP on bone physiology. The aim of the present study was to assess whether stable GIP analogues were capable of ameliorating bone strength in mice with diet-induced obesity. The stable GIP analogue (D-Ala^2)-GIP, and (D-Ala^2)-GIP-Tag, a specific GIP analogue homing exclusively to bone, were employed. *In vitro* studies were used to assess effects of (D-Ala^2)-GIP and (D-Ala^2)-GIP-Tag on bone mineralization, lysyl oxidase activity, collagen maturity as well as osteoclast formation and activity. Subsequent *in vivo* studies employed obese-prediabetic Swiss NIH mice subjected to a 42-day period of daily administration of saline, (D-Ala^2)-GIP or (D-Ala^2)-GIP-Tag. *In vitro* studies confirmed that (D-Ala^2)-GIP and (D-Ala^2)-GIP-Tag had similar beneficial biological effects on bone cells. Administration of (D-Ala^2)-GIP and (D-Ala^2)-GIP-Tag resulted in lower blood glucose levels without any effects on body weight. Both GIP analogues augmented bone strength to a similar extent. Trabecular or cortical bone microarchitecture were not changed over the time course of the study. However, (D-Ala^2)-GIP and (D-Ala^2)-GIP-Tag augmented enzymatic collagen crosslinking as well as the heterogeneity of enzymatic collagen crosslinking, mineral-to-matrix ratio and significantly reduced the heterogeneity in mineral bone crystallite size. This study demonstrates that activation of skeletal GIPr by stable GIP analogues enhance bone strength in prediabetes and suggest that these analogues may be beneficial in the treatment of bone disease.

Keywords: GIP-Tag, bone fragility, bone composition, type 2 diabetes

1. INTRODUCTION

The burden of diabetes is progressing worldwide at an alarming rate. It is projected that by 2045 there will be an estimated number of 629 million individuals with diabetes [1]. Diabetes is associated with comorbidities including micro- and macrovascular complications, peripheral neuropathy and bone fractures. Indeed, diabetes is associated with a higher risk of bone fractures at the hip and at the spine, despite higher or normal bone mineral densities at these two sites [2-5].

The resistance of bone to fracture depends on bone mass, i.e., the quantity of bone, but also on the organization of the bone matrix at the structural and tissue levels. Alterations of both cortical and trabecular bone microarchitectures have been linked to decreased bone strength. Bone composition is also an important contributor of bone strength. The bone matrix is comprised of an organic layer, composed mainly of type I collagen, proteoglycans and non-collagenous protein [6]. This organic layer serves as a template for the nucleation and growth of poorly crystalline hydroxyapatite and the subsequent mineralization of bone matrix. Both the organic and mineral layers are important for bone strength, and alterations in either of these components leads to changes in bone strength.

Glucose-dependent insulinotropic polypeptide (GIP) is produced and secreted by enteroendocrine K-cells, located mostly in the duodenum [7]. Whilst in the circulation, GIP can access several target organs such as the pancreas where it stimulates insulin secretion from beta pancreatic cells [8]. Physiologically GIP is one of the two incretin hormones responsible for potentiation of insulin secretion following feeding [9]. We previously reported beneficial effects of several gut hormones on bone strength in diabetes [10-13]. However, the possible effects of GIP analogues have not been reported to date. Due to its role as the major physiological incretin hormone, GIP effects on bone are interesting to test in diabetes.

Deletion of GIP receptor (GIPr) in mice leads to a skeletal phenotype with deterioration of cortical bone microarchitecture, alterations of both mineral and collagen component of the bone matrix and ultimately lower bone strength [14-17]. Administration of the long-acting, N-AcGIP analogue in rats, led to ameliorations of bone strength due to improvement in bone composition [18]. The GIPr is expressed by bone cells (osteoblasts and osteoclasts) and culture of GIP analogues with bone cells enhances osteoblast function and reduces osteoclast formation and activation [19, 20]. In humans, GIP also exerts anti-resorptive effects [21, 22] and a polymorphism of the GIPr has been linked to higher risk of developing non vertebral bone fractures [23].

GIPr are found in extra-skeletal tissues, and it is therefore unclear whether the beneficial effects on bone are due to direct activation of bone cells or by indirect action on extra-skeletal organs that are responsible for better bone strength. To overcome this problem, we developed a novel GIP analogue that exhibits specific bone tropism [24]. This analogue, called GIP-Tag, has N-terminal enzymatic protection by substitution of L-Ala^2 with D-Ala^2, together with six aspartic acids at its C-terminal extremity that confers affinity for bone mineral. We have previously shown that GIP-Tag exhibits comparable binding activity at the GIPr and activates similar intracellular pathways in bone cells as the parent GIP peptide [24].

Recent works highlighted the dramatic bone fragility resulting from high fat diet on bone strength and quality [11, 12] and as such, the aim of the present study was to evidence whether GIP-Tag was capable of enhancing osteoblast mineralization and collagen post-processing *in vitro*, and to assess whether GIP-Tag was capable of ameliorating bone strength in a diet-induced obesity rodent model.

2. MATERIAL AND METHODS

2.1. Peptide characterization

(D-Ala^2)-GIP and (D-Ala^2)-GIP-Tag were synthesized and purchased from EZ Biolabs Ltd (Carmel, IN, USA) at >95% purity. Peptides were further characterized in-house by reverse phase high performance liquid chromatography after dissolution in water using a Kinetex C-18 HPLC analytical column (150 x 4.6 mm, Phenomenex, Cheshire, UK). Equilibration of the column was performed with 0.1% (v/v) TFA/water at a flow rate of 1 ml/min. Linear acetonitrile gradients (0-70% in 40 mins) were used for elution and absorbance measured at 214 nm. The molecular mass of peptides was confirmed using a Voyager-DE biospectrometry workstation (PerSeptive Biosystems, Farmingham, MA, USA). Dipeptidyl peptidase-4 (DPP-4) mediated degradation of the peptides was assessed as described by Gault et al [25]. Briefly, 30 µg peptides were incubated with 5 mU porcine DPP-4 in 50 mM triethanolamine hydrochloride (TEA, pH 7.8) at 37°C for 0, 2, 8, 12 and 24 h. The enzymatic reaction was then stopped using 50 µl TFA/water (10% v/v). Degradation profiles were determined using HPLC and degradation products were analyzed by mass spectrometry.

2.2. Cell culture

MC3T3-E1 cells are phenotypically normal osteoblasts derived from foetal mouse calvaria and differentiate in culture resulting ultimately to the formation of a bone-like extracellular matrix [26]. MC3T3-E1 cells were purchased from American Type Culture Collection (ATCC, Teddington, UK). Cells were grown and expanded at a ratio 1:4 in propagation medium containing αMEM supplemented with 10% FBS, 100 U/mL penicillin, and 100 µg/mL streptomycin in a humidified atmosphere enriched with 5% CO_2 at 37°C. For differentiation studies, cells were detached with trypsin-EDTA and plated at a density of 1.5×10^4 cells/cm^2 and grown to confluence in propagation medium. At confluence, the propagation medium was replaced by differentiation medium containing αMEM supplemented with 10% FBS, 100 U/mL penicillin, 100 µg/mL streptomycin, 3.5 g/L D-glucose (final glucose concentration 4.5 g/L), 50 µg/ml ascorbic acid, 2.5 mM Na_2HPO_4 and 100 pM peptide. The differentiation medium was replenished every two days. At the end of the 13-day culture period, cells were either fixed with 3.7% (w/v) formaldehyde in PBS for 10 minutes (mineralization assay) or absolute ethanol (collagen maturity assay). For the mineralization assay, the cell layer was then rinsed with PBS and stained with 1% (w/v) alizarin red S for 5 minutes. The plates were then rinsed three times with 50% ethanol and left to air dry. An image of the full well was made by light microscopy by inverting the plate on the microscope stage. The extent of mineralization was assessed by image analysis with ImageJ 1.52p (National Institutes of Health, Bethesda, MA, USA). A lower grey level indicates a higher mineralization.

2.3. Lysyl oxidase (LOX) activity

LOX activity was assessed in the cell culture supernatants and in the cell layers after 13 days of culture. This period of time was chosen as it corresponds to the highest expression of LOX [27] using a fluorometric assay developed by Palamakumbura et al. [28]. At day 12, the differentiation medium was replaced by phenol red-free DMEM containing 0.5% bovine serum albumin, 50 µg/ml ascorbic acid, 2.5 mM Na_2HPO_4 and 100 pM peptide. After 24 hrs, cell culture supernatants were collected, centrifuged at 3000 rpm for 30 min at 4°C, aliquoted and stored at -80°C until use. The cell layer was extracted in urea buffer as reported previously [29]. Samples (supernatant, cell layer extract) were then incubated at 37°C for 30 minutes in the presence of 1.2 M urea, 50 mM sodium borate (pH 8.2), 1.3 nmol H_2O_2, 1 UI/ml horseradish peroxidase, 10 mM diaminopentane, 10 µM Ampliflu™ red and ± 0.5 mM beta-aminopropionitrile (BAPN) in opaque 96-well plates. At the end of the incubation period, plates were placed on ice and fluorescence was read using a M2 microplate reader (Molecular devices, St Gregoire,

France) with excitation and emission wavelengths set up at 563 nm and 587 nm, respectively. As BAPN is a specific LOX inhibitor, the residual amine oxidase activity evidenced in the presence of BAPN was subtracted from the activity observed in the absence of BAPN. LOX activity was reported as the fold change versus CTRL of the pooled supernatant and cell layer fractions.

2.4. Osteoclast generation from human peripheral blood mononuclear cells

Peripheral blood mononuclear cells (PBMCs) were isolated from the buffy coat of healthy individuals (Etablissement français du sang, Angers, France) as reported previously [30]. In order to generate osteoclasts, PBMCs cells were plated at a concentration of 1 x 10^6 cells/cm^2 in 24-well plate or on top of dentine slices in alpha-MEM supplemented with 10% fetal calf serum, 2 mM L-glutamine, 100 U/ml penicillin, 100 μg/ml streptomycin, 50 ng/ml sRANKL (Bio-techne) and 10 nM of GIP analogues. This concentration of GIP was used based on previous published data [20]. All factors were replenished every 2-3 days. After 14 days of culture, the expression of tartrate resistant acid phosphatase (TRAP) was examined histochemically in 24-well plate. Briefly, cells were rinsed promptly in PBS buffer, fixed with formalin (10% in PBS buffer) for 10 minutes and rinsed in distilled water. TRAP was demonstrated histochemically by a simultaneous coupling reaction using Naphtol AS-BI-phosphate as substrate and Fast violet B as the diazonium salt. Cells were then incubated for 90 minutes at 37°C in the dark, rinsed three times in distilled water and the residual activity was inhibited by 4% NaF for 30 minutes. Cells were then rinsed in distilled water, counterstained with DAPI for 20 minutes and allowed to dry. TRAP positive cells, with more than three nuclei, were identified as osteoclasts. Furthermore, after 21 days in culture, the dentine slices were removed from the culture wells, placed in NH_4OH (1N) for 30 minutes and sonicated for 5 minutes to remove any adherent cells. After rinsing in distilled water, the dentine slices were stained with 0.5% (v/v) toluidine blue (pH 5.0) prior to examination by light microscopy. The extent of surface erosion were determined using imageJ.

2.5. Animals

All procedures were conducted in accordance with UK Home Office Regulations (UK Animals Scientific Procedures Act 1986) and in compliance with the ARRIVE guidelines [31]. Male NIH Swiss mice (NIH/OlaHsd) were obtained from Envigo Ltd (Blackthorn, UK) at 8 weeks of age. Animals were individually housed in an air-conditioned room at 22 ± 2°C with a 12-hour light/dark cycle, and had free access to tap water and high fat diet (45% fat, 20% protein, 35% carbohydrate; Special Diet Service,

Essex, UK) *ad libitum* for 90 days prior to the start of the study. High fat fed (HFF) mice (n=6) were divided in three groups and received once daily (09:30 h) intraperitoneal (i.p.) injections of: (1) saline (0.9% NaCl – HFD+saline), (2) (D-Ala^2)-GIP (25 nmol/kg bw) and (3) (D-Ala^2)-GIP-Tag (25 nmol/kg bw), with both peptides delivered in saline vehicle. This dosing regimen was chosen based on our previous experience with related gut-derived peptides in high fat fed mice [12, 32, 33]. Pharmacological intervention was continued for 42 consecutive days. No adverse effects were observed following peptide treatment. Body weight and blood glucose concentrations were measured at regular intervals, blood was withdrawn at approximately 10:00 h on appropriate days. An i.p. glucose tolerance test (18 mmol/kg bw) was performed following an 18 hour fast on day 43. All blood samples were collected from the tail vein of animals and glucose measured using a portable Bayer Ascencia Counter blood glucose meter (Bayer Healthcare, Newbury, Berkshire, UK). At necropsy, femurs and tibias were cleaned of soft tissues and stored in 70% ethanol at 4°C until used.

2.6. MicroCT

MicroCT analyses were performed on tibias with a Skyscan 1272 microtomograph (Bruker MicroCT, Kontich, Belgium) operated at 70 kV, 140 µA, 1000-ms integration time. The isotropic pixel size was fixed at 4 µm, the rotation step at 0.25° and exposure was performed with a 0.5-mm aluminum filter. Each 3D reconstruction image dataset was binarized using global thresholding. Trabecular volume of interest (VOI) was located 0.5-mm below the growth plate and extended on 2-mm. Cortical volume of interest extended on 1-mm centered at the midshaft tibia. All histomorphometrical parameters were determined using the CTan software (version 1.17.7.2, Bruker microCT) according to guidelines and nomenclature proposed by the American Society for Bone and Mineral Research [34].

2.7. Bone strength assessment

Three-point bending experiments were performed on femurs after rehydrating bones at 4°C for 24 h. Femurs were loaded to failure in 3-point bending at 1 mm/min using an Instron 5942 (Instron, Elancourt, France). The lower span length was set to 10 mm. Femurs were oriented so the anterior quadrant was facing down and subjected to tensile loads. For each bone, load and displacement were digitally recorded at a sampling rate of 100 Hz and measured using a 500 N load cell (Instron). The load-displacement curve was computed with the Bluehill 3 software (Instron) and the maximum load, yield

load (0.2% offset method), stiffness, post-yield displacement and work to failure were computerized. After three-point bending experiments, distal parts of femur were embedded undecalcified in polymethylmethacrylate (pMMA) at 4°C.

2.8. Fourier-transform infrared microspectroscopy/imaging (FTIRM/FTIRI)

For collagen cross-link analysis (collagen maturity), osteoblast cultures were fixed in absolute ethanol as indicated above, scrapped off the culture dish and transferred onto BaF_2 windows where they were air-dried. Integrity of the collagen extracellular matrix was verified by comparing the obtained FTIRM spectrum with those of commercial collagen. Spectral analyses were performed using a Bruker Vertex 70 spectrometer (Bruker optics, Ettlingen, Germany) interfaced with a Bruker Hyperion 3000 infrared microscope equipped with a standard single element Mercury Cadmium Telluride (MCT) detector. Infrared spectra were recorded at a resolution of 4 cm^{-1}, with an average of 32 scans in transmission mode. Background spectral images were collected under identical conditions from the same BaF_2 windows at the beginning and end of each experiment to ensure instrument stability. For FTIRM analysis, 20 spectra were acquired for each condition. Each spectrum was corrected for Mie scattering with the RMieS-EMSC_v5 algorithm (kind gift of Prof Peter Gardner, University of Manchester, UK). Spectra were vector normalized for the amide I band, second derivative spectroscopy was applied to find the position of underlying peaks in the amide I band and curve fitting was performed with a routine script in Matlab (The Mathworks, Natick, USA). Collagen maturity was determined as the relative ratio of pyridinium trivalent (Pyr, mature collagen) to dehydrodihydroxylysinonorleucine divalent (deH-DHLNL, new collagen) collagen cross-links using their respective subbands located at 1660 cm^{-1} and 1690 cm^{-1} of the amide I peak [35, 36].

For analysis of *in vivo* samples, cross-sectional sections (4 µm) of the midshaft femur were sandwiched between barium fluoride optical windows. FTIRI was performed with the same spectrometer and microscope but with a focal plane array detector (64 x 64 pixels) covering a field of view of 180 x 180 µm. Nine consecutive field-of-views were stitched together to allow sufficient bone to be analyzed. Sections were scanned with a spectral resolution of 8 cm^{-1} (spectral region 900-2000 cm^{-1}). Each spectrum was corrected for Mie scattering. Prior to pMMA subtraction, the area of the 1715 - 1745 cm^{-1} peak, corresponding to the C=O vibration of pMMA, and the amide I band, located between 1590-1710

cm^{-1} were computed. After pMMA subtraction, spectrum were vector normalized for the v1,v3 phosphate band analyzed with a routine script in Matlab (The Mathworks, Natick, USA) as previously reported [37]. The evaluated infrared spectral parameters were: (1) Tissue water content, calculated as the area ratio of the pMMA peak (1715-1745 cm^{-1}) to amide I (1590-1710 cm^{-1}), both computed before pMMA subtraction. This ratio represents a surrogate to water content in the bone matrix [38]. (2) mineral/matrix ratio (area of υ1, υ3 phosphate/area amide1); (3) acid phosphate content (intensity ratio 1127cm^{-1}/1096 cm^{-1}); (4) mineral maturity (intensity ratio 1030 cm^{-1}/1020 cm^{-1}), reflecting crystal size and perfection; (5) crystal size index (intensity ratio 1075 cm^{-1}/1055 cm^{-1}), reflecting crystal size in 002, 211, 200 and 202 directions [39]; (6) carbonate/phosphate ratio (intensity υ3 carbonate located at ~1415 cm^{-1}/1030 cm^{-1}) was computed after subtracting the organic matrix spectrum [40]; and (7) collagen maturity (intensity ratio 1660 cm^{-1}/1690 cm^{-1}). Histogram distribution for each compositional parameter was fitted with a Gaussian model and considered normally distributed if the R^2 coefficient was >0.95. In the present study, none of the histograms deviated from normal distribution. For each of the compositional parameters, the mean and full width at half maximum of the pixel distribution (excluding the zero background values) were computed and represented as mean and heterogeneity.

2.9. Statistical analysis

All data were analyzed using Prism 6.0 (GraphPad Software Inc, La Jolla, CA). Kruskal-Wallis with Dunn's multiple comparisons tests were employed to test for significance when otherwise stated. Two-way ANOVA with Tukey multiple comparison tests were used to assess significant differences in body weight and blood glucose. Multiple regression analyses were performed with Systat 13 (Systat software, San Jose, CA, USA). Differences at p equal to or less than 0.05 were considered significant. Data are presented as median ± interquartile range.

3. RESULTS

3.1. (D-Ala^2)-GIP-Tag and (D-Ala^2)-GIP acted similarly on bone cells *in vitro*

Initially, as expected, we confirmed that both (D-Ala^2)-GIP and (D-Ala^2)-GIP-Tag were resistant to DPP-4 mediated degradation (data not shown) as both peptides were still intact after a 8-h incubation with DPP-4. We previously observed that (D-Ala^2)-GIP and (D-Ala^2)-GIP-Tag exhibited similar bone related responses in the presence of 1 g/L glucose [24]. However, little was known about the response in the

presence of elevated glucose concentration. We assessed the extent of mineralization in the presence of 4.5 g/L glucose. As seen in Figure 1A, (D-Ala²)-GIP and (D-Ala²)-GIP-Tag significantly increased mineral deposition in the cultures. Furthermore, (D-Ala²)-GIP and (D-Ala²)-GIP-Tag significantly increased LOX activity, responsible for enzymatic collagen crosslinking (Fig. 1B). Indeed, collagen maturity, expressed as the ratio of mature/immature collagen crosslinks, was significantly augmented by 42% ($p=0.026$) and 43% ($p=0.021$) in (D-Ala²)-GIP- and (D-Ala²)-GIP-Tag-treated cultures, respectively. We next examined whether (D-Ala²)-GIP and (D-Ala²)-GIP-Tag were capable of reducing human osteoclast formation and activity *in vitro*. Human peripheral mononuclear cells were differentiated in the presence of (D-Ala²)-GIP or (D-Ala²)-GIP-Tag. As shown in Figures 1C-D, (D-Ala²)-GIP was capable of reducing osteoclast formation by 24% ($p=0.022$) and activity by 26% ($p=0.014$). Similarly, (D-Ala²)-GIP-Tag reduced osteoclast formation by 27% ($p=0.027$) and osteoclast-mediated bone resorption by 32% ($p=0.018$). No significant differences between the two pharmacological interventions were evident in any of the *in vitro* parameters studied.

3.2. (D-Ala²)-GIP and (D-Ala²)-GIP-Tag improved blood glucose and bone strength

As (D-Ala²)-GIP and (D-Ala²)-GIP-Tag were both active *in vitro*, we decided to administer these two peptides to high fat fed (HFF) animals. Previously, we reported that HFF animals presented with alterations of bone mechanical resistance, as well as deterioration not only in trabecular and cortical bone microarchitectures, but also in the mineral and organic components of bone matrix [11, 12]. HFF mice were characterized by increased body weight and elevated blood glucose. We first investigated therefore whether (D-Ala²)-GIP and (D-Ala²)-GIP-Tag affected these parameters. Body weight was not significantly modified during the 42 days administration of (D-Ala²)-GIP or (D-Ala²)-GIP-tag (Figure 2A). However, non-fasting blood glucose levels were significantly reduced after 42 days of treatment with (D-Ala²)-GIP and (D-Ala²)-GIP-Tag, respectively (Figure 2B). Interestingly, glucose levels following a glucose challenge on day 42 were reduced in (D-Ala²)-GIP ($p<0.001$) and (D-Ala²)-GIP-Tag ($p=0.001$) mice at 105 min post-injection, with glucose-lowering effects more prominent in (D-Ala²)-GIP treated mice (Figure 2 C-D). Corresponding glucose-induced insulin concentrations were not significantly different between all groups of HFF mice (data now shown). We also examined whether bone mechanical response was modified by peptide administration in HFF mice. Ultimate load was significantly increased by 13% ($p=0.024$) and 10% ($p=0.041$) with (D-Ala²)-GIP and (D-Ala²)-GIP-Tag,

respectively (Figure 3). Work-to-fracture, representing the energy required to break the bone, was significantly augmented by 30% (p=0.004) and 20% (p=0.037) with (D-Ala²)-GIP and (D-Ala²)-GIP-Tag, respectively. On the other hand, stiffness and post-yield displacement were not significantly different between the three groups of animals.

3.3. (D-Ala²)-GIP and (D-Ala²)-GIP-Tag had no effects on bone microarchitecture

As mechanical response depends on structural and compositional properties, we assessed trabecular and cortical bone microarchitectures. Figure 4A represents 3D-models of tibia proximal metaphysis in saline-, (D-Ala²)-GIP- and (D-Ala²)-GIP-Tag-treated animals. No obvious differences could be detected between the three groups. Quantification of histomorphometrical parameters did not evidence any significant modifications of either trabecular or cortical bone microarchitecture (Figures 4B-C).

3.4. (D-Ala²)-GIP and (D-Ala²)-GIP-Tag effects on bone composition

We next examined whether pharmacological intervention with (D-Ala²)-GIP and (D-Ala²)-GIP-Tag modified the composition of the bone matrix. Each compositional parameters is described by its average quantity (mean) and heterogeneity (width). As reported in Figure 5, (D-Ala²)-GIP significantly augmented XLR-mean, XLR-width and MM-mean. On the other hand, (D-Ala²)-GIP significantly reduced TWC-mean and CSI-width. None of the other compositional parameters were affected by (D-Ala²)-GIP administration. (D-Ala²)-GIP-Tag significantly augmented XLR-mean, XLR-width and MM-mean in the bone matrix, and reduced CSI-width. However, (D-Ala²)-GIP-Tag treatment failed to modify tissue water content. Multiple regression analyses highlighted the importance of modifications of collagen maturity (mean and heterogeneity) in the changes in ultimate load and work-to-fracture (Table 1).

4. DISCUSSION

Bone fragility is recognized as a comorbidity of type 2 diabetes mellitus, which has been suggested to improve with better glycemic control. However, as some glucose-lowering therapies have previously been shown to increase fracture risk [41], it is a prerequisite to assess the safety and potential beneficial effects of such pharmacological interventions. GIP is an established incretin hormone, but it also makes an important contribution to bone strength [14, 15]. In the present manuscript we have evaluated the effects of GIP analogue therapies on bone strength in a rodent model of diet-induced obesity. We

compared two GIP analogues: the native peptide with a D-alanine in position 2, as well as this stable GIP analogue with an additional C-terminal modification of 6 aspartic acid residues, conferring a bone tropism and called GIP-Tag [24]. As evident from the present results, both peptides were capable of increasing bone matrix mineralization and maturity *in vitro*, but also reduced osteoclast activation in the presence of high glucose concentration (equivalent to 25 mmol/L), suggesting that these peptides might present with interesting properties to prevent fragility fracture in diabetes. These observations are in agreement with previous published literature showing a reduction of bone resorption following GIP infusion in humans, which seems independent of glycemia [22]. Interestingly, the addition of the aspartic residues Tag at the C-terminus of GIP did not appear to affect its biological activity. Previously, we have shown GIP-Tag to exhibit similar binding activities at the GIP receptor as (D-Ala²)-GIP or GIP_{1-42} [24]. Furthermore, activation of intracellular pathways such as adenylate cyclase, intracellular calcium, p38α, CREB, AMPKα2 and STAT2 have been evidenced with parent and GIP-Tag peptides [24].

In the present study, administration of (D-Ala²)-GIP and (D-Ala²)-GIP-Tag to obese pre-diabetic animals, resulted in higher ultimate bending load and work-to-fracture with no modifications of cortical (and trabecular) bone microarchitecture. This suggests that improved bone strength was due to modifications of bone tissue composition. This is very interesting when compared with the effects of exenatide, a known GLP-1 mimetic that not only improved mechanical strength but also induced changes in cortical bone microarchitecture and bone tissue composition [12].

Multiple regression analysis suggested that ultimate load and work-to-fracture were associated with changes in collagen maturity, but none of other changes in bone tissue composition. This observation shows the limit of studying tissue composition by Fourier transform infrared imaging. Thus, although it is indicative of changes in several bone composition parameters, changes in bone composition do not ultimately result in positive modifications of bone strength at the whole bone level.

Blood glucose levels were decreased at the end of the study by both GIP analogues. With respect to the incretin action of GIP, it is not surprising to observe such effects with (D-Ala²)-GIP, although assessment of circulating insulin concentrations would be required to confirm this. However, the effect of (D-Ala²)-GIP-Tag that rapidly homes to bone, is perhaps surprising and suggests the possibility that some bone-produced factors are responsible for the control of glycemia. In this regard, development of specific assays to assess the pharmacokinetic profile of (D-Ala²)-GIP and (D-Ala²)-GIP-Tag would be interesting, but beyond the scope of the current study. In addition, it is worth noting that glucose-induced

insulin secretion was not altered by either of the treatments. One related factor could be osteocalcin, which has been shown to function as an insulin secretagogue [42, 43]. However, previous reports suggested that GIP reduced osteocalcin expression and translation [44]. This area will require further investigation in the future. Whether a GIP-osteocalcin reciprocal relationship exists, as observed with GLP-1 [45, 46], will also require more detailed study.

The similarity between the effects of (D-Ala^2)-GIP and (D-Ala^2)-GIP-Tag suggest that skeletal GIP receptors are required for beneficial effects of GIP on bone properties. This is in contrast to what was seen in ovariectomy-induced bone loss and osteopenia as (D-Ala^2)-GIP-Tag was far less effective than (D-Ala^2)-GIP in enhancing bone strength and quality [24]. However, another possible scenario would be represented by the amelioration of the glycemic profile with both peptides, and it is possible that the beneficial effects on bone are not represented by direct action of GIP on bone parameters but rather by reduction of the negative effects of chronic hyperglycemia. Further studies are required to fully ascertain the mechanism behind the beneficial bone effects. In addition, the impact of both treatments of GIP secretion, and ambient endogenous GIP levels, would be interesting to consider in follow-up investigations.

In conclusion, this study has demonstrated the potential of GIP analogues not just in the treatment of diet-induced obesity and prediabetes, but also to improve bone strength through effects on bone tissue composition. Further studies in humans are required to ascertain whether GIP analogues might represent a viable option in preventing bone fragility in diabetes.

5. ACKNOWLEDGEMENTS

The authors are grateful to Nadine Gaborit and Stéphanie Lemière (University of Angers, GEROM-LHEA, Institut de Biologie en Santé, Angers, France) for their help with microCT. This work was supported by grants from the Irish Endocrine Society as well as University of Ulster Research Challenge Fund and Proof of Principle Funding Programs.

6. REFERENCES

[1] I.D. Federation, IDF Diabetes Atlas - 8th edition, 2017.

[2] A.V. Schwartz, D.E. Sellmeyer, K.E. Ensrud, J.A. Cauley, H.K. Tabor, P.J. Schreiner, S.A. Jamal, D.M. Black, S.R. Cummings, G. Study of Osteoporotic Features Research, Older women with

diabetes have an increased risk of fracture: a prospective study, J Clin Endocrinol Metab 86(1) (2001) 32-38.

[3] P. Vestergaard, Discrepancies in bone mineral density and fracture risk in patients with type 1 and type 2 diabetes--a meta-analysis, Osteoporos Int 18(4) (2007) 427-344.

[4] D.E. Bonds, J.C. Larson, A.V. Schwartz, E.S. Strotmeyer, J. Robbins, B.L. Rodriguez, K.C. Johnson, K.L. Margolis, Risk of fracture in women with type 2 diabetes: the Women's Health Initiative Observational Study, J Clin Endocrinol Metab 91(9) (2006) 3404-3410.

[5] N. Napoli, A.V. Schwartz, A.L. Schafer, E. Vittinghoff, P.M. Cawthon, N. Parimi, E. Orwoll, E.S. Strotmeyer, A.R. Hoffman, E. Barrett-Connor, D.M. Black, G. Osteoporotic Fractures in Men Study Research, Vertebral Fracture Risk in Diabetic Elderly Men: The MrOS Study, J Bone Miner Res 33(1) (2018) 63-69.

[6] A.L. Boskey, P.G. Robey, The composition of bone, in: J.P. Bilezikian (Ed.), Primer on the metabolic bone diseases and disorders of mineral metabolism, John Wiley & Sons, Inc, Hoboken, NJ, USA, 2018.

[7] A.M. Habib, P. Richards, L.S. Cairns, G.J. Rogers, C.A. Bannon, H.E. Parker, T.C. Morley, G.S. Yeo, F. Reimann, F.M. Gribble, Overlap of endocrine hormone expression in the mouse intestine revealed by transcriptional profiling and flow cytometry, Endocrinology 153(7) (2012) 3054-3065.

[8] L.L. Baggio, D.J. Drucker, Biology of incretins: GLP-1 and GIP, Gastroenterology 132(6) (2007) 2131-2157.

[9] M.A. Nauck, J.J. Meier, Incretin hormones: Their role in health and disease, Diabetes Obes Metab 20 Suppl 1 (2018) 5-21.

[10] S.A. Mansur, A. Mieczkowska, P.R. Flatt, B. Bouvard, D. Chappard, N. Irwin, G. Mabilleau, A new stable GIP-Oxyntomodulin hybrid peptide improved bone strength both at the organ and tissue levels in genetically-inherited type 2 diabetes mellitus, Bone 87 (2016) 102-113.

[11] S.A. Mansur, A. Mieczkowska, P.R. Flatt, D. Chappard, N. Irwin, G. Mabilleau, Sitagliptin Alters Bone Composition in High-Fat-Fed Mice, Calcif Tissue Int 104(4) (2019) 437-448.

[12] S.A. Mansur, A. Mieczkowska, P.R. Flatt, D. Chappard, N. Irwin, G. Mabilleau, The GLP-1 Receptor Agonist Exenatide Ameliorates Bone Composition and Tissue Material Properties in High Fat Fed Diabetic Mice, Front Endocrinol 10 (2019) 51.

[13] M. Pereira, S. Gohin, J.P. Roux, A. Fisher, M.E. Cleasby, G. Mabilleau, C. Chenu, Exenatide Improves Bone Quality in a Murine Model of Genetically Inherited Type 2 Diabetes Mellitus, Front Endocrinol 8 (2017) 327.

[14] C. Gaudin-Audrain, N. Irwin, S. Mansur, P.R. Flatt, B. Thorens, M. Basle, D. Chappard, G. Mabilleau, Glucose-dependent insulinotropic polypeptide receptor deficiency leads to modifications of trabecular bone volume and quality in mice, Bone 53(1) (2013) 221-230.

[15] A. Mieczkowska, N. Irwin, P.R. Flatt, D. Chappard, G. Mabilleau, Glucose-dependent insulinotropic polypeptide (GIP) receptor deletion leads to reduced bone strength and quality, Bone 56(2) (2013) 337-342.

[16] K. Tsukiyama, Y. Yamada, C. Yamada, N. Harada, Y. Kawasaki, M. Ogura, K. Bessho, M. Li, N. Amizuka, M. Sato, N. Udagawa, N. Takahashi, K. Tanaka, Y. Oiso, Y. Seino, Gastric inhibitory polypeptide as an endogenous factor promoting new bone formation after food ingestion, Mol Endocrinol 20(7) (2006) 1644-1651.

[17] D. Xie, H. Cheng, M. Hamrick, Q. Zhong, K.H. Ding, D. Correa, S. Williams, A. Mulloy, W. Bollag, R.J. Bollag, R.R. Runner, J.C. McPherson, K. Insogna, C.M. Isales, Glucose-dependent insulinotropic polypeptide receptor knockout mice have altered bone turnover, Bone 37(6) (2005) 759-769.

[18] G. Mabilleau, A. Mieczkowska, N. Irwin, Y. Simon, M. Audran, P.R. Flatt, D. Chappard, Beneficial effects of a N-terminally modified GIP agonist on tissue-level bone material properties, Bone 63 (2014) 61-68.

[19] A. Mieczkowska, B. Bouvard, D. Chappard, G. Mabilleau, Glucose-dependent insulinotropic polypeptide (GIP) directly affects collagen fibril diameter and collagen cross-linking in osteoblast cultures, Bone 74 (2015) 29-36.

[20] G. Mabilleau, R. Perrot, A. Mieczkowska, S. Boni, P.R. Flatt, N. Irwin, D. Chappard, Glucose-dependent insulinotropic polypeptide (GIP) dose-dependently reduces osteoclast differentiation and resorption, Bone 91 (2016) 102-112.

[21] A. Nissen, M. Christensen, F.K. Knop, T. Vilsboll, J.J. Holst, B. Hartmann, Glucose-dependent insulinotropic polypeptide inhibits bone resorption in humans, J Clin Endocrinol Metab 99(11) (2014) E2325-E2329.

[22] M.B. Christensen, A. Lund, S. Calanna, N.R. Jorgensen, J.J. Holst, T. Vilsboll, F.K. Knop, Glucose-Dependent Insulinotropic Polypeptide (GIP) Inhibits Bone Resorption Independently of Insulin and Glycemia, J Clin Endocrinol Metab 103(1) (2018) 288-294.

[23] S.S. Torekov, T. Harslof, L. Rejnmark, P. Eiken, J.B. Jensen, A.P. Herman, T. Hansen, O. Pedersen, J.J. Holst, B.L. Langdahl, A functional amino acid substitution in the glucose-dependent insulinotropic polypeptide receptor (GIPR) gene is associated with lower bone mineral density and increased fracture risk, J Clin Endocrinol Metab 99(4) (2014) E729-E733.

[24] G. Mabilleau, B. Gobron, A. Mieczkowska, R. Perrot, D. Chappard, Efficacy of targeting bone-specific GIP receptor in ovariectomy-induced bone loss, J Endocrinol 239(2) (2018) 215-227.

[25] V.A. Gault, P.R. Flatt, C.J. Bailey, P. Harriott, B. Greer, M.H. Mooney, P. O'Harte F, Enhanced cAMP generation and insulin-releasing potency of two novel Tyr1-modified enzyme-resistant forms of glucose-dependent insulinotropic polypeptide is associated with significant antihyperglycaemic activity in spontaneous obesity-diabetes, Biochem J 367(Pt 3) (2002) 913-920.

[26] R.T. Franceschi, B.S. Iyer, Y. Cui, Effects of ascorbic acid on collagen matrix formation and osteoblast differentiation in murine MC3T3-E1 cells, J Bone Miner Res 9(6) (1994) 843-854.

[27] H.H. Hong, N. Pischon, R.B. Santana, A.H. Palamakumbura, H.B. Chase, D. Gantz, Y. Guo, M.I. Uzel, D. Ma, P.C. Trackman, A role for lysyl oxidase regulation in the control of normal collagen deposition in differentiating osteoblast cultures, J Cell Physiol 200(1) (2004) 53-62.

[28] A.H. Palamakumbura, P.C. Trackman, A fluorometric assay for detection of lysyl oxidase enzyme activity in biological samples, Anal Biochem 300(2) (2002) 245-251.

[29] D. Bedell-Hogan, P. Trackman, W. Abrams, J. Rosenbloom, H. Kagan, Oxidation, cross-linking, and insolubilization of recombinant tropoelastin by purified lysyl oxidase, J Biol Chem 268(14) (1993) 10345-10350.

[30] G. Mabilleau, D. Chappard, A. Sabokbar, Role of the A20-TRAF6 axis in lipopolysaccharide-mediated osteoclastogenesis, J Biol Chem 286(5) (2011) 3242-3249.

[31] C. Kilkenny, W.J. Browne, I.C. Cuthill, M. Emerson, D.G. Altman, Improving bioscience research reporting: the ARRIVE guidelines for reporting animal research, PLoS Biol 8(6) (2010) e1000412.

[32] N. Irwin, P.L. McClean, K. Hunter, P.R. Flatt, Metabolic effects of sustained activation of the GLP-1 receptor alone and in combination with background GIP receptor antagonism in high fat-fed mice, Diabetes Obes Metab 11(6) (2009) 603-610.

[33] C.M. Martin, N. Irwin, P.R. Flatt, V.A. Gault, A novel acylated form of (d-Ala(2))GIP with improved antidiabetic potential, lacking effect on body fat stores, Biochim Biophys Acta 1830(6) (2013) 3407-3413.

[34] M.L. Bouxsein, S.K. Boyd, B.A. Christiansen, R.E. Guldberg, K.J. Jepsen, R. Muller, Guidelines for assessment of bone microstructure in rodents using micro-computed tomography, J Bone Miner Res 25(7) (2010) 1468-1486.

[35] E.P. Paschalis, S. Gamsjaeger, D.N. Tatakis, N. Hassler, S.P. Robins, K. Klaushofer, Fourier Transform Infrared Spectroscopic Characterization of Mineralizing Type I Collagen Enzymatic Trivalent Cross-Links, Calcif Tissue Int 96(1) (2015) 18-29.

[36] E.P. Paschalis, K. Verdelis, S.B. Doty, A.L. Boskey, R. Mendelsohn, M. Yamauchi, Spectroscopic characterization of collagen cross-links in bone, J Bone Miner Res 16(10) (2001) 1821-8.

[37] E. Aguado, G. Mabilleau, E. Goyenvalle, D. Chappard, Hypodynamia Alters Bone Quality and Trabecular Microarchitecture, Calcif Tissue Int 100(4) (2017) 332-340.

[38] E.P. Paschalis, P. Fratzl, S. Gamsjaeger, N. Hassler, W. Brozek, E.F. Eriksen, F. Rauch, F.H. Glorieux, E. Shane, D. Dempster, A. Cohen, R. Recker, K. Klaushofer, Aging Versus Postmenopausal Osteoporosis: Bone Composition and Maturation Kinetics at Actively-Forming Trabecular Surfaces of Female Subjects Aged 1 to 84 Years, J Bone Miner Res 31(2) (2016) 347-357.

[39] S.J. Gadaleta, E.P. Paschalis, F. Betts, R. Mendelsohn, A.L. Boskey, Fourier transform infrared spectroscopy of the solution-mediated conversion of amorphous calcium phosphate to hydroxyapatite: new correlations between X-ray diffraction and infrared data, Calcif Tissue Int 58(1) (1996) 9-16.

[40] H. Ou-Yang, E.P. Paschalis, W.E. Mayo, A.L. Boskey, R. Mendelsohn, Infrared microscopic imaging of bone: spatial distribution of CO3(2-), J Bone Miner Res 16(5) (2001) 893-900.

[41] A.V. Schwartz, Diabetes, bone and glucose-lowering agents: clinical outcomes, Diabetologia 60(7) (2017) 1170-1179.

[42] N.K. Lee, H. Sowa, E. Hinoi, M. Ferron, J.D. Ahn, C. Confavreux, R. Dacquin, P.J. Mee, M.D. McKee, D.Y. Jung, Z. Zhang, J.K. Kim, F. Mauvais-Jarvis, P. Ducy, G. Karsenty, Endocrine regulation of energy metabolism by the skeleton, Cell 130(3) (2007) 456-469.

[43] M. Ferron, E. Hinoi, G. Karsenty, P. Ducy, Osteocalcin differentially regulates beta cell and adipocyte gene expression and affects the development of metabolic diseases in wild-type mice, Proc Natl Acad Sci U S A 105(13) (2008) 5266-5270.

[44] S. Kainuma, H. Tokuda, K. Fujita, T. Kawabata, G. Sakai, R. Matsushima-Nishiwaki, A. Harada, O. Kozawa, T. Otsuka, Attenuation by incretins of thyroid hormone-stimulated osteocalcin synthesis in osteoblasts, Biomed Rep 5(6) (2016) 771-775.

[45] A. Mizokami, Y. Yasutake, S. Higashi, T. Kawakubo-Yasukochi, S. Chishaki, I. Takahashi, H. Takeuchi, M. Hirata, Oral administration of osteocalcin improves glucose utilization by stimulating glucagon-like peptide-1 secretion, Bone 69 (2014) 68-79.

[46] A. Mizokami, Y. Yasutake, J. Gao, M. Matsuda, I. Takahashi, H. Takeuchi, M. Hirata, Osteocalcin induces release of glucagon-like peptide-1 and thereby stimulates insulin secretion in mice, PLoS One 8(2) (2013) e57375.

7. FIGURE LEGENDS

Figure 1 [On-line color only]: Effects of (D-Ala²)-GIP or (D-Ala²)-GIP-Tag on bone cells *in vitro*. MC3T3-E1 cells were differentiated in the presence of ascorbic acid, Na_2HPO_4 and a final glucose concentration of 25 mM in the presence of vehicle, (D-Ala²)-GIP or (D-Ala²)-GIP-Tag. (A) Mineralization extent (B) lysyl oxidase activity and (C) enzymatic collagen crosslinking in the extracellular matrix. Peripheral blood mononuclear cells were also differentiated in osteoclasts in the presence of vehicle, (D-Ala²)-GIP or (D-Ala²)-GIP-Tag. (D) Number of newly-formed osteoclasts/well and (E) extent of surface resorption by differentiated osteoclasts. Vehicle: white bars, (D-Ala²)-GIP: black bars, (D-Ala²)-GIP-Tag: grey bars. *: $p<0.05$ vs. vehicle-treated cultures. Data are presented as median ± interquartile range from 3-5 independent experiments.

Figure 2 [On-line color only]: Metabolic parameters at the beginning and end of the 42 days period of pharmacological intervention. (A) Body weight and (B) blood glucose were assessed three days before administering vehicle or peptides and then every three days during the 42-day period of the study. (C) Blood glucose was measured prior to and after i.p. administration of glucose (18 mmol/kg) at t = 0 min on day 43 in fasted animals and (D) incremental area under the glucose curves (AUC) between 0 and 105 min was computed. *: $p<0.05$ vs. saline-treated animals. NS: not significant. Data are presented as median ± interquartile range for n=6/group.

Figure 3 [On-line color only]: Effects of (D-Ala²)-GIP or (D-Ala²)-GIP-Tag on bone mechanical resistance. Biomechanical response of femurs was tested by three-point bending. (A) Ultimate load, (B) Stiffness, (C) Post-yield displacement (PYD) and (D) Work-to-fracture. Saline: white bars, (D-Ala²)-GIP: black bars, (D-Ala²)-GIP-Tag: grey bars. *: $p<0.05$ vs. saline-treated animals. Data are presented as median ± interquartile range for n=6/group.

Figure 4 [On-line color only]: Effects of (D-Ala²)-GIP or (D-Ala²)-GIP-Tag on bone structural properties. Tibias were scanned by high resolution X-ray microcomputed tomography and trabecular and cortical bone microarchitecture were evaluated in the proximal metaphysis. (A) Three-dimensional reconstruction of proximal metaphysis, (B) trabecular and (C) cortical bone parameters. BV/TV: trabecular bone volume density, Tb.N: trabecular number, Tb.Th: trabecular thickness, Tb.Sp: trabecular separation, Tt.Ar: total tissue area, Ma.Ar: Marrow area, Ct.Ar: cortical bone area, Ct.Th:

cortical thickness. Saline: white bars, (D-Ala²)-GIP: black bars, (D-Ala²)-GIP-Tag: grey bars. Data are presented as median ± interquartile range for n=6/group.

Figure 5 [On-line color only]: Effects of (D-Ala²)-GIP and (D-Ala²)-GIP-Tag on bone matrix composition. The composition of the mineral and organic phase of the bone matrix was evaluated by Fourier transform infrared imaging. The distribution of each parameter over the bone frequency area was computed and curve fitted with a Gaussian curve. The average and full width at half maximum of the Gaussian distribution were also calculated for each parameter and presented as “mean” and “width”. XLR: collagen maturity, XST: mineral crystallinity, CSI: crystal size index, MM: mineral-to-matrix ratio, C/P: carbonate content, Ac.P: acid phosphate content, TWC: tissue water content, CG: collagen glycation. Saline: white bars, (D-Ala²)-GIP: black bars, (D-Ala²)-GIP-Tag: grey bars. *: $p<0.05$ vs. saline-treated animals. Data are presented as median ± interquartile range for n=6/group.

8. TABLES

Table 1: Multiple regression analyses between bone compositional and mechanical parameters.

Dependent variable	Model adjusted R^2	Model p value	Parameter	Coefficient	p value
Ultimate load	0.846	<0.001	Intercept	-45.6	0.015
			XLR_mean	25.1	0.022
Work-to-fracture	0.408	0.033	XLR_width	14.435	0.033

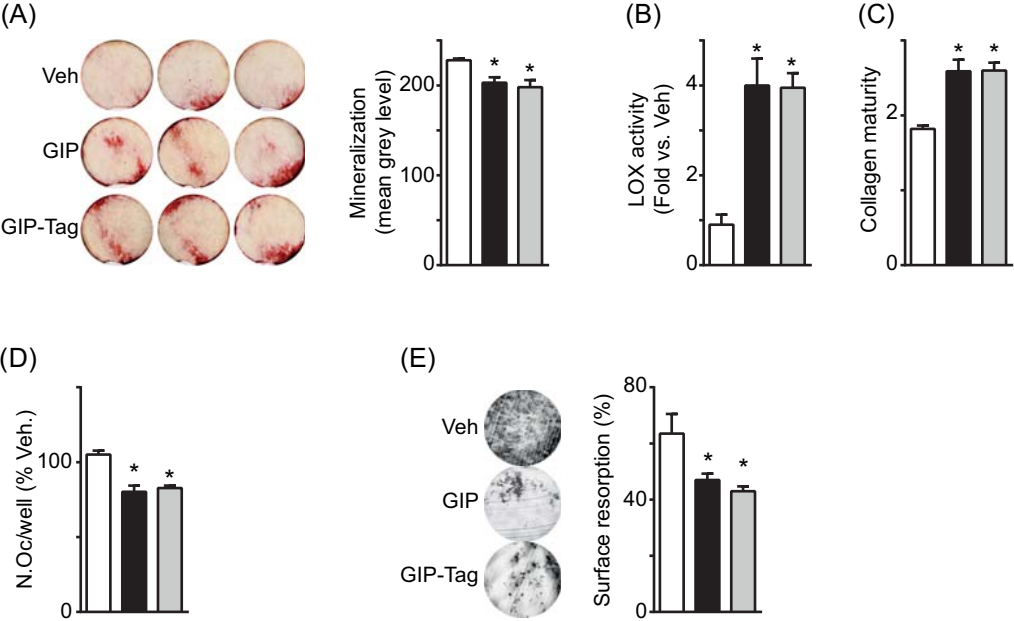
(A)
Veh
GIP
GIP-Tag
Mineralization (mean grey level)
200
100
0
*
*
(B)
LOX activity (Fold vs. Veh)
4
2
0
*
*
(C)
Collagen maturity
2
0
*
*
(D)
N.Oc/well (% Veh.)
100
0
*
*
(E)
Veh
GIP
GIP-Tag
Surface resorption (%)
80
40
0
*
*

Figure 1

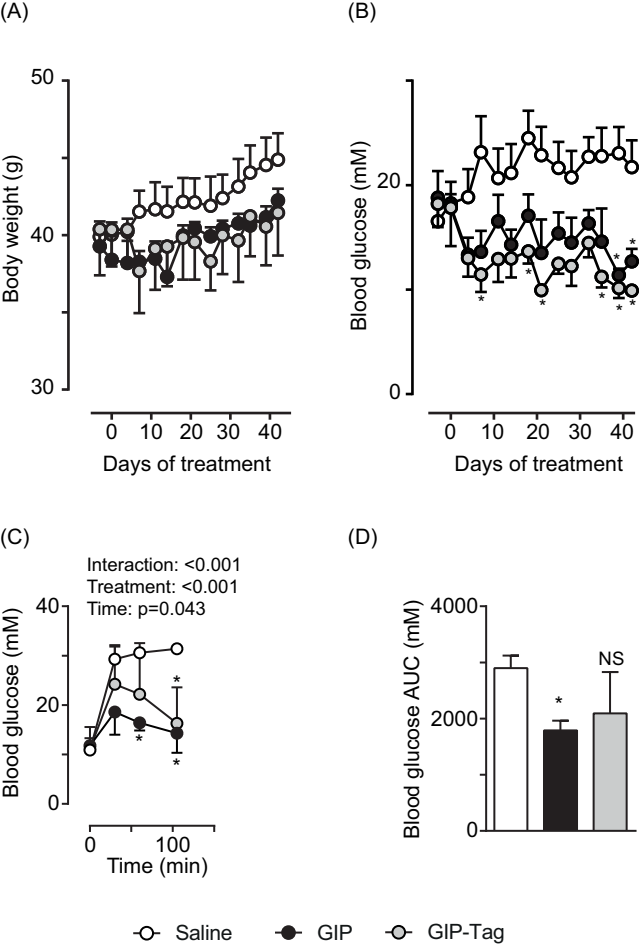
(A)
Body weight (g)
50
40
30
0 10 20 30 40
Days of treatment
(B)
Blood glucose (mM)
20
0
0 10 20 30 40
Days of treatment
(C)
Interaction: <0.001
Treatment: <0.001
Time: p=0.043
Blood glucose (mM)
40
20
0
0 100
Time (min)
(D)
Blood glucose AUC (mM)
4000
2000
0
NS
Saline
GIP
GIP-Tag

Figure 2

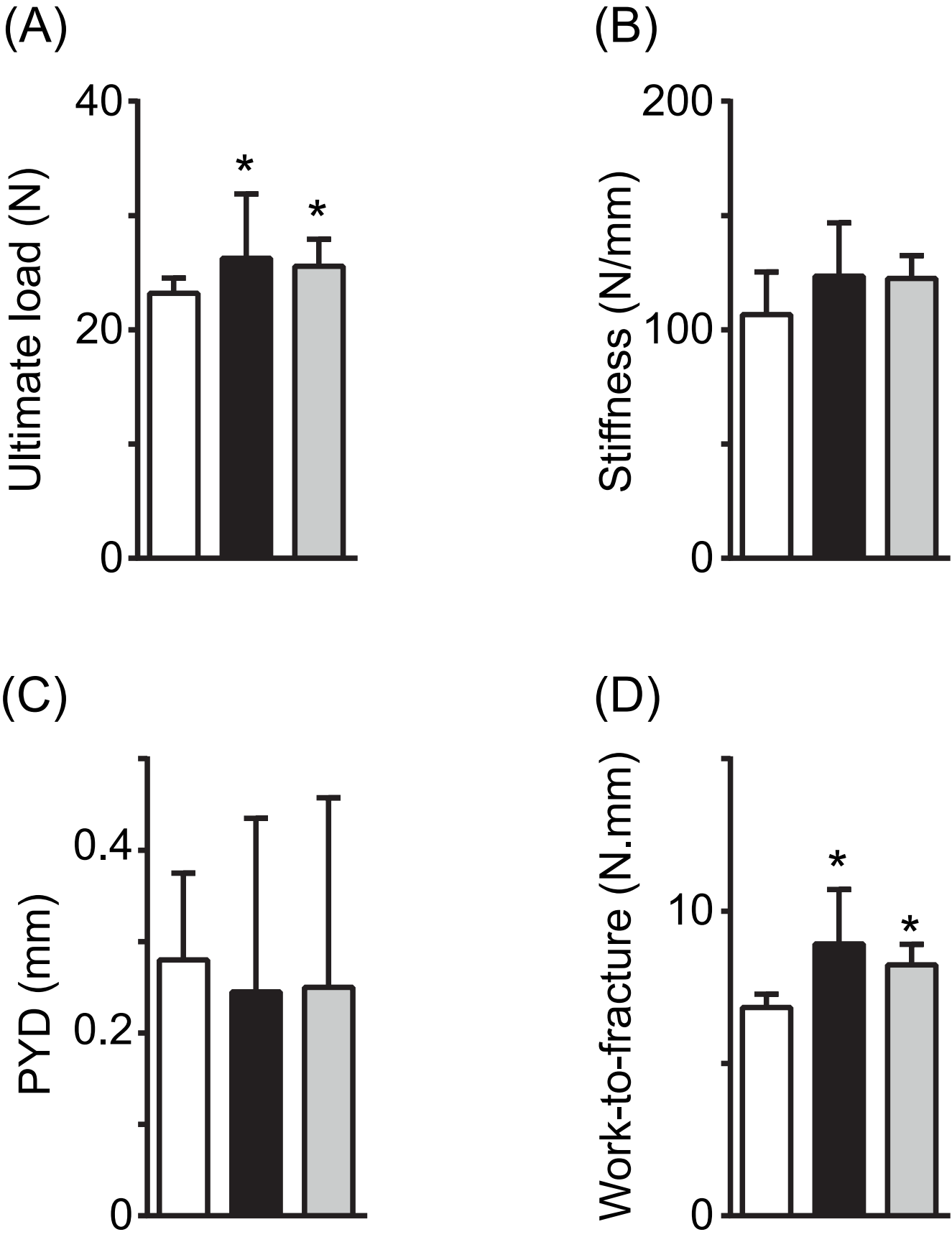
(A)
Ultimate load (N)
40
20
0
*
*
(B)
Stiffness (N/mm)
200
100
0
(C)
PYD (mm)
0.4
0.2
0
(D)
Work-to-fracture (N.mm)
10
0
*
*

Figure 3

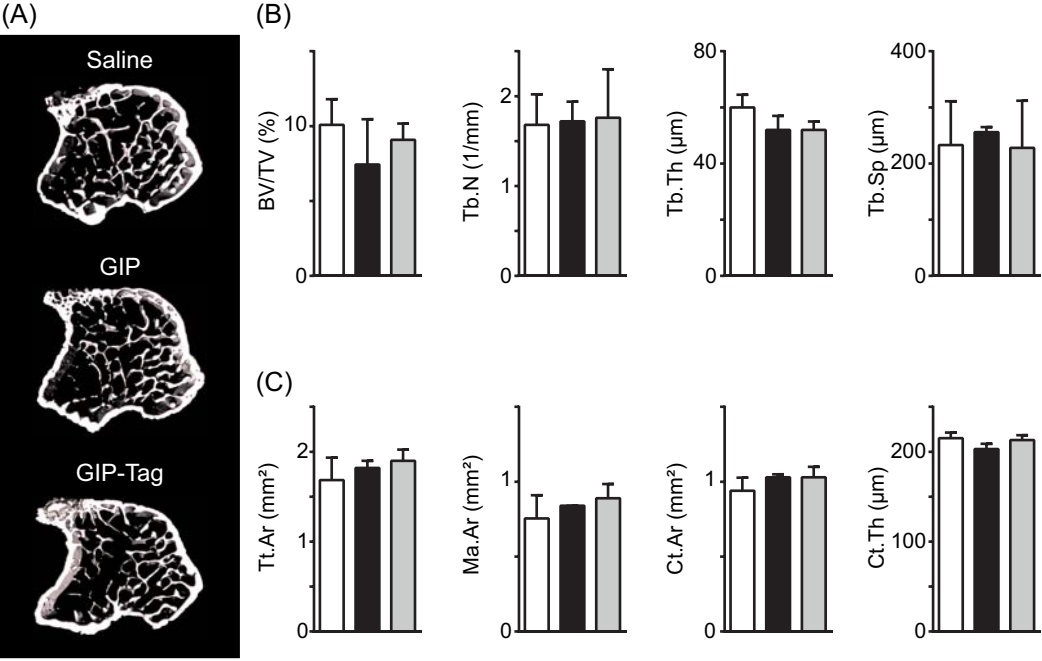
(A)
Saline
GIP
GIP-Tag
(B)
BV/TV (%)
10
0
Tb.N (1/mm)
2
1
0
Tb.Th (μm)
80
40
0
Tb.Sp (μm)
400
200
0
(C)
Tt.Ar (mm²)
2
1
0
Ma.Ar (mm²)
1
0
Ct.Ar (mm²)
1
0
Ct.Th (μm)
200
100
0

Figure 4

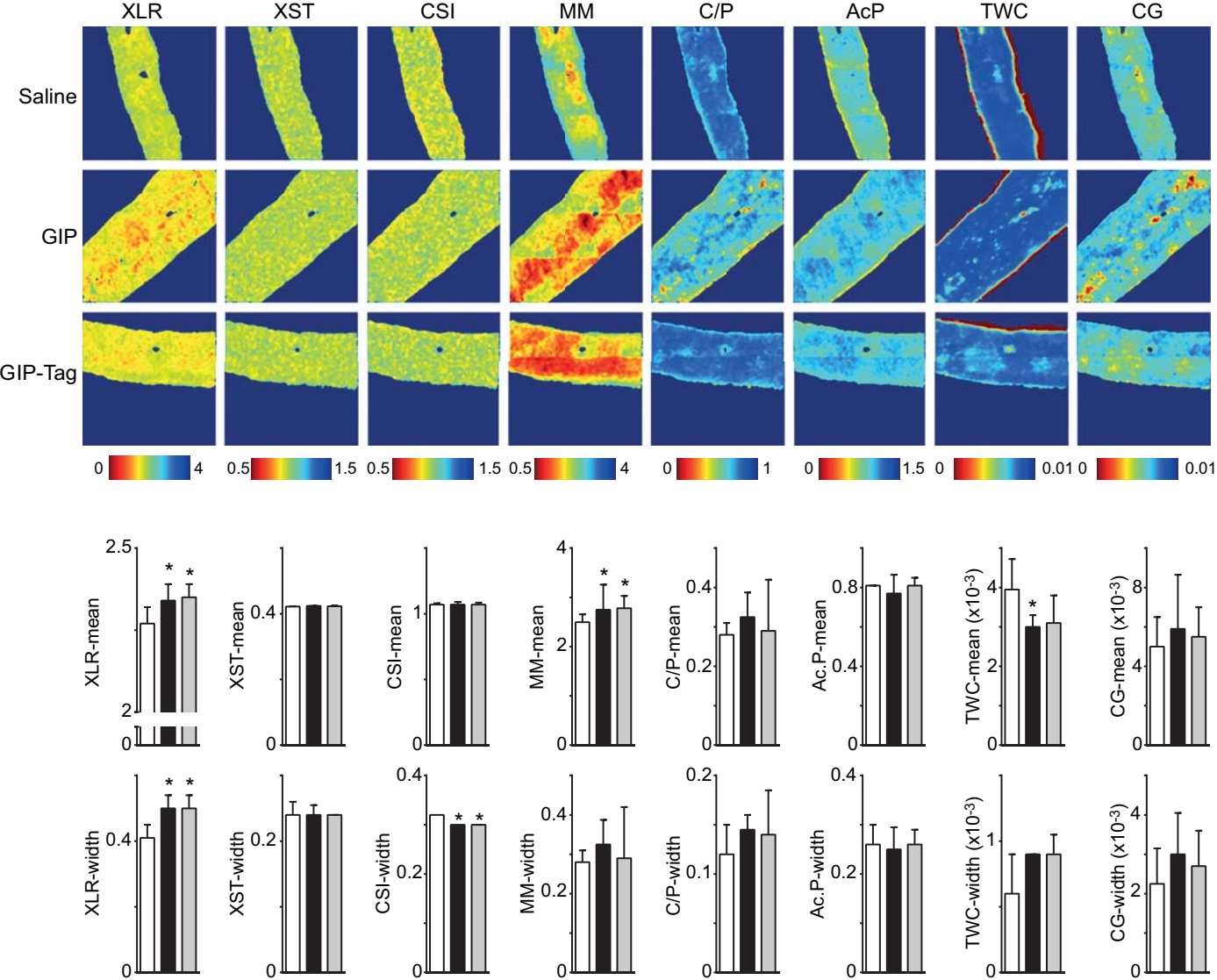
XLR
XST
CSI
MM
C/P
AcP
TWC
CG
Saline
GIP
GIP-Tag
0 4
0.5 1.5
0.5 1.5
0.5 4
0 1
0 1.5
0 0.01
0 0.01
XLR-mean
XST-mean
CSI-mean
MM-mean
C/P-mean
Ac.P-mean
TWC-mean (x10-3)
CG-mean (x10-3)
XLR-width
XST-width
CSI-width
MM-width
C/P-width
Ac.P-width
TWC-width (x10-3)
CG-width (x10-3)

Figure 5